Supporting Online Material for

Atomic View of a Toxic Amyloid Small Oligomer

Arthur Laganowsky, Cong Liu, Michael R. Sawaya, Julian P. Whitelegge, Jiyong Park, Minglei Zhao, Anna Pensalfini, Angela Soriaga, Meytal Landau, Poh K. Teng, Duilio Cascio, Charles Glabe, David Eisenberg

correspondence to: david@mbi.ucla.edu

This PDF file includes:

Materials and Methods

Peptide Crystallization

Synthetic peptides were purchased from CS BIO (Menlo Park, CA). All peptides were filtered through a 0.22 μm Ultrafree-MC centrifugal filter device (AMICON, Bedford, MA, USA) prior to crystallization in hanging drop plates. All crystallization was performed at room temperature. KVKVLGDVIEV (K11V, see Table S1) was dissolved in water to a final concentration of 10 mM and mixed with 5 mM OrangeG (Product No. 861286, Sigma-Aldrich, St. Louis, MO), for a final concentration of 4 mM K11V and 3 mM OrangeG. This peptide mixture was crystallized in 0.1 M BIS-TRIS (pH 6.5), 45% 2-methyl-2,4-pentanediol (MPD), 0.2 M ammonium acetate (Index #51, Hampton Research, Aliso Viejo, CA). K11V-Br2, (2-Bromoallyl)-glycine substitution at position 2, was dissolved in water at 15 mg/mL, crystallized in 0.1 M TRIS (pH 7.0), 35% MPD, 0.2 M sodium chloride (Wizard #24, Emerald BioSystems, Bainbridge Island, WA) and crystals appeared in 1-3 days. K11V-Br8, (2-bromoallyl)-glycine substitution at position 8, was dissolved in water at 15 mg/mL and crystallized in 0.1 M HEPES (pH 7.5), 30% MPD, 0.2 M sodium citratre tribasic dihydrate (Crystal Screen #5, Hampton Research, Aliso Viejo, CA). KLKVLGDVIEV ($K11V^{V2L}$) was dissolved in water at 10-15 mg/mL and crystallized in 0.1M TRIS (pH 7.0), 35% MPD, 0.2M sodium chloride (Wizard #24, Emerald BioSystems, Bainbridge Island, WA). GDVIEV (G6V) was dissolved in water at 6 mg/mL and crystallized in 2.1 M DL-Malic acid pH 7.0 ($JCSG^{+}$ #68, Qiagen, Valencia, CA).

Recombinant Beta Cylindrin Tandem Repeat Peptide Plasmid Construction

A tandem repeat beta cylindrin peptide, K11V-TR, synthetic gene, codon optimized for *E. coli*, was designed using DNAWorks (*51*) and constructed using PCR-based gene synthesis as described (*51*). The synthetic gene was PCR amplified with Platinum Pfx polymerase (Invitrogen, Carlsbad, CA) with the N-terminal primer containing a SacI restriction and TEV protease site, and a C-terminal primer containing a stop codon and XhoI restriction site. Agarose gel purified PCR product, K11V-TR, was extracted using the QIAquick Gel Extraction Kit (Qiagen, Valencia, CA). Gel purified PCR product and custom vector, p15-MBP (described below), were digested with SacI and XhoI according to manufacturer's protocol (New England Biolabs, Ipswich, MA). The p15-MBP custom vector is a chimera constructed from the NdeI and XhoI digestion products pET15b (Novagen, Gibbstown, NJ), and the maltose binding protein (MBP) gene from pMAL-C2X (New England Biolabs, Ipswich, MA), resulting in an N- terminal His-tag MBP fusion vector. Digested vector products were gel purified and extracted (as described above). DNA concentrations were determined using BioPhotometer UV/VIS Photometer (Eppendorf, Westbury, NY). A ligation mixture was performed using a Quick Ligation kit (New England Biolabs, Ipswich, MA) according to manufacturer protocol and transformed into *E. coli* cell line TOP10 (Invitrogen, Carlsbad, CA). Several colonies were grown overnight, and plasmid containing the synthetic K11V-TR gene were purified using QIAprep Spin Miniprep Kit (Qiagen, Valencia, CA). The final construct

p15-MBP-K11V-TR was sequenced prior to transformation into *E. coli* expression cell line BL21 (DE3) gold cells (Agilent Technologies, Santa Clara, CA).

Recombinant Beta Cylindrin Peptide Mutant Constructs

All mutations in the DNA sequence were performed on the p15-MBP-K11V-TR plasmid using a Site-Directed Mutagenesis kit (QuickChange XL, Stratagene, La Jolla, CA) with site-directed primers designed using manufacturers QuickChange Primer Design Program available on-line (Stratagene, La Jolla, CA) according to manufacturer's protocol. The $K11V^{V2L}$ construct was achieved by mutation of the first glycine residue coding sequence in the linker region to a stop codon. The $K11V^{V4W}$-TR was achieved by two-rounds of site-directed mutagenesis. The final constructs were sequenced prior to transformation into *E. coli* expression cell line BL21 (DE3) gold cells (Agilent Technologies, Santa Clara, CA).

Recombinant Beta Cylindrin Peptide Expression

A single colony was inoculated into 50 mL LB Miller broth (Fisher Scientific, Pittsburgh, PA) supplemented with 100 µg/mL ampicillin (Fisher Scientific, Pittsburgh, PA) and grown overnight at 37 ˚C. One liter of LB Miller supplemented with 100 µg/mL ampicillin in 2L shaker flasks was inoculated with 7 mL of overnight culture and grown at 37 ˚C until the culture reached an OD600 ~0.6-0.8 using a BioPhotometer UV/VIS Photometer (Eppendorf, Westbury, NY). IPTG (Isopropyl β–D-1-thiogalactopyranoside) was added to a final concentration of 0.5 mM, and grown for 3-4 hours at 34 ˚C. Cells were harvested by centrifugation at 5,000 x g for 10 minutes at 4 ˚C. The cell pellet was frozen and stored at -80 ˚C.

Recombinant Beta Cylindrin Peptide Purification

The cell pellet was thawed on ice and re-suspended in buffer A (50 mM sodium phosphate, 0.3 M sodium chloride, 20 mM imidazole, pH 8.0) supplemented with Halt Protease Inhibitor Cocktail (Thermo Scientific, Rockford, IL) at 50 mL per 2L of culture volume. The re-suspended culture was incubated on ice for 15 minutes prior to sonication. Crude cell lysate was clarified by centrifugation at 14,000 x g for 25 minutes at 4 ˚C. The clarified cell lysate was filtered through a 0.45 µm syringe filtration device (HPF Millex-HV, Millipore, Billerica, MA) before loading onto a 5mL HisTrap-HP column (GE Healthcare, Piscataway, NJ). The HisTrap-HP column was washed with five column volumes of buffer A and protein eluted with linear gradient to 100% in four column volumes of buffer B (50 mM sodium phosphate, 0.3 M sodium chloride, 500 mM imidazole, pH 8.0). Protein eluted around 50-70% buffer B and peak fractions pooled. A final concentration of 5 mM beta-mercaptoethanol (BME) and 1 mM ethylenediaminetetraacetic acid (EDTA) was added to the pooled sample prior to transferring to a Slide-A-Lyzer 10,000 MWCO dialysis cassette (Pierce, Thermo Fisher Scientific, Rockford, IL), and dialyzed against buffer C (25 mM sodium phosphate pH 8.0, 20 mM imidazole, 200 mM sodium chloride) at room temperature overnight. The dialyzed sample was pooled and 1/500 volume of TEV protease stock (*16*) was added. The TEV protease reaction was incubated overnight at room temperature before loading over a 5mL HisTrap-HP column equilibrated in buffer A. The flow through was

collected, containing the recombinant beta cylindrin peptide with an additional N-terminal glycine residue resulting from TEV protease cleavage. Pooled recombinant beta cylindrin peptide was 0.22 µm filtered (Steriflip, Millipore, Billerica, MA) and further purified by reverse phase high performance liquid chromatography (RP-HPLC) on a 2.2 x 25 cm Vydac 214TP101522 column equilibrated in buffer RA (0.1% trifluroacetic acid (TFA)/water) and eluted over a linear gradient from 0% to 100% buffer RB (Acetonitrile/0.1% TFA) in 40 minutes at a flow rate of 9 mL/min. Absorbance at 220nm and 280nm were recorded using a Waters 2487 dual ʎ absorbance detector (Waters, Milford, MA). Peak fractions containing peptide were assessed for purity by either a MALDI-TOF mass spectrometry (Voyager-DE-STR, Applied Biosystems, Carlsbad, CA) or direct infusion nanoelectrospray mass spectrometry using a hybrid linear ion-trap/FT-ICR mass spectrometer (7T, LTQ FT Ultra, Thermo Scientific, Bremen, Germany). Pooled fractions were frozen in liquid nitrogen and lyophilized. Dried peptide powders were stored in desiccant jars at -20 °C.

Size Exclusion Chromatography HPLC (SEC-HPLC)

One to five milligrams of lyophilized peptide was dissolved in 1mL of water and filtered through a 0.22 or 0.45 µm Centrex MF filter (Whatman, Florham Park, NJ). Filtered samples were injected on a 21.5 mm x 60 cm Tosohaas G3000SW column (Tosoh Bioscience, King of Prussia, PA) equilibrated in SEC buffer (25mM sodium phosphate, 100mM sodium sulfate pH 6.5) at a flow rate of 3 mL/min. Absorbance at 220nm and 280nm were recorded using a Waters 2487 dual ʎ absorbance detector (Waters, Milford, MA). Protein standards were monitored by absorbance at 280nm, and cylindrin peptides monitored by absorbance at 220nm. For native nanoelectrospray mass spectrometry experiments the SEC buffer was changed to 200 mM ammonium acetate, pH adjusted to 6.5 with acetic acid.

Recombinant K11V-TR Beta Cylindrin Peptide Crystallization

Crystals of K11V-TR were grown in hanging drop VDX plates (Hampton Research, Aliso, Viejo, CA) from either (i) purified oligomeric complexes or (ii) freshly dissolved peptide preparations. i) Peak fractions from SEC-HPLC in SEC buffer containing the oligomeric K11V-TR complex was concentrated using a 3,500 MWCO concentrator (Millipore, Billerica, MA) at 4 °C. The concentrated K11V-TR buffer was exchanged by several washes in buffer (100mM sodium chloride, 20 mM HEPES pH 7.5) followed by concentration. The buffer exchanged K11V-TR complex was concentrated to a concentration of ~2.5 mg/mL, as judged by the Bradford assay (Bio-Rad, Hercules, CA) using known solutions of K11V-TR for a standard curve. ii) A microfuge tube containing a pre-weighed quantity of K11V-TR, usually a few milligrams, was chilled on ice. A given volume of ice cold water was gently added to yield a final peptide concentration of 2.5 mg/mL, and stored on ice until dissolution of peptide was complete without disturbance. Both preparations of the K11V-TR complex were either used immediately or stored at 4 °C prior to use. Crystals of K11V-TR were grown using ice cold components of a K11V-TR preparation with crystallization solution 30% MPD, 0.2M magnesium acetate, 0.1M sodium cacodylate pH 6.5 (Crystal Screen #21, Hampton

Research, Aliso Viejo, CA). Crystallization was carried out at 10 °C. Crystals from either starting preparations displayed similar X-ray diffraction quality.

X-ray Diffraction Data Collection

All data were collected at 100K at Advanced Light Source (Berkeley, CA) beam line 8.2.1, Advanced Photon Source (Chicago, IL) beam lines 24-ID-C and 24-ID-E, and in-house on a Rigaku Raxis-IV++ imaging plate detector using Cu K(alpha) radiation from a Rigaku FRE+ rotating anode generator with confocal optics (Table S2). Single crystals were mounted with CrystalCap HT Cryoloops (Hampton Research, Aliso Viejo, CA). K11V, K11V^{V2L}, K11V-Br2, K11V-Br8, and K11V-TR crystals were flash frozen in liquid nitrogen prior to data collection. For experimental phases, K11V-TR crystals were soaked briefly in a mother liquor solution containing potassium iodide and flash frozen in liquid nitrogen. G6V crystals were cryoprotected in mother liquor solution containing 20% glycerol and flash frozen in liquid nitrogen.

X-ray Diffraction Data Processing and Refinement

All data were processed using DENZO (*52*) and SCALEPACK (*52*) or XDS (*53*). G6V initial phases were found by molecular replacement of a poly-alanine beta sheet template peptide. K11V-Br2 and K11V-Br8 were phased using HKL2MAP (*54*), and models built using COOT (*55*). K11V and K11V^{V2L} were phased by molecular replacement using PHASER (*56*) with the K11V-Br2 structure. Low resolution (~2.9 Å) experimental phases for K11V-TR was obtained from iodo soaked crystal diffraction data collected in-house using HKL2MAP (*54*), and followed by model building using COOT (*55*). All model refinement was done using REFMAC (*57*) and PHENIX (*58*).

Surface Area Buried and Surface Complementarity Calculations

Surface area (*59*) and shape complementarity (*60*) calculations were performed with AREAIMOL and SC programs distributed by CCP4 (*61*).

Native Nanoelectrospray Mass Spectrometry

Peak fractions containing the K11V-TR complex from SEC-HPLC in buffer (0.2M ammonium acetate, pH 6.5) were analyzed by direct nanospray injection (for review see (*62*)). Fractions were individually loaded into a 2-μm internal diameter externally coated nanospray emitter (ES380, Thermo) and desorbed by adjusting the spray voltage to maintain an ion current between 0.1 and 0.2 μA. A hybrid linear ion-trap/FTICR mass spectrometer was used for the analysis (7T, LTQ FT Ultra, Thermo Scientific, Bremen, Germany). Individual charge states of multiply protonated K11V-TR complex ions were selected for isolation and collisional activation in the linear ion trap followed by detection of the resulting product ions in the FTICR cell. Xtract software (Thermo Scientific, Bremen, Germany) was used to compute monoisotopic mass from the measured isotopomer profile.

Dot Blot Analysis

Briefly, a small aliquot of cylindrin peptide samples, at a concentration of a few mg/mL, were spotted onto a nitrocellulose membrane (Trans-Blot, Bio-Rad, Hercules,

CA). After blocking with 10% fat free milk in TBST buffer (50 mM Tris, 150 mM NaCl, 0.05% Tween20), the membranes were incubated with polyclonal antibody or monoclonal antibody (~1:250 dilution in 5% fat free milk, TBST buffer) at room temperature for 1 hour. The membranes were washed three times in TBST buffer before incubating with anti-rabbit HRP-linked antibody (1:5000 dilution in 5% fat free milk, TBST buffer) (Invitrogen, Carlsbad, CA) at room temperature for 1 hour. After washing the membranes three times in TBST buffer, the films were developed following the protocol as described in the Kit (Thermo Scientific Pierce ECL Western Blotting Substrate, #32209). Positive controls for A11 and OC were prefibrillar oligomers and fibrils, respectively (*5*).

Fibril Formation and Electron Microscopy

Fibrillation assays were initially carried out in fifteen different fibrillation conditions, then narrowed down to four conditions: A – phosphate buffered saline, B – 25mM TRIS pH 8.5, 150mM sodium chloride, C – 10% dimethyl sulfoxide (DMSO), 25mM TRIS pH 8.5, 150mM sodium chloride, and D – 10mM CAPS pH 11.0, 150mM sodium chloride, 1mM EDTA. Beta cylindrin peptides stock solutions (10mg/mL in water) were diluted in a fibrillation buffer to a final concentration of 1 mg/mL in a microfuge. Samples were incubated at 50 °C with vigorous shaking (Torrey Pines Scientific, Carlsbad, CA) for one week. Most cylindrin peptides grew fibrils in buffer D, and some in buffers B-C. Fibrils did not appear in buffer A, but served as a negative control.

Cell Culture and Viability Assay

Cell viability was investigated using a CellTiter 96 aqueous non-radioactive cell proliferation assay kit (MTT) (Promega cat. #G4100). SH-SY5Y (ATCC; cat. # CRL-2266), PC-12(ATCC; cat. # CRL-1721), HeLa and HEK293 were used to assess the toxic effect of clyindrin peptides. HeLa and HEK293 cells were cultured in DMEM medium with 10% fetal bovine serum. SH-SY5Y cells were cultured in F12/DMEM 1:1 medium with 10% fetal bovine serum, PC-12 cells were cultured in ATCC-formulated RPMI 1640 medium (ATCC; cat.# 30-2001) with 10% heat-inactivated horse serum and 5% fetal bovine serum. Cells were maintained at 37 °C in 5% CO_2. For all toxicity experiments, 96-well plates (Costar cat. # 3596) were used. HeLa, HEK293 and PC-12 cells were plated out at 10,000 cells per well and SH-SY5Y cells were plated at 25,000 cells per well. Cells were cultured for 20h at 37 °C in 5% CO_2 prior to addition of peptide samples. 10 µl of sample was added to each well containing 90 µL medium, and allowed to incubate for 24h prior to adding 15 µl Dye solution (Promega. cat. #G4102) into each well, followed by incubation for 4h at 37°C in 5% CO_2. After incubation, 100 µl solubilization Solution/Stop Mix (Promega cat. #G4101) was added to each well. After 12h incubation at room temperature, the absorbance was measured at 570nm. Background absorbance was recorded at 700nm. Each of the experiments was repeated 3 times with 4 replicates per sample per concentration. The concentration for cylindrin peptides were based on their oligomeric state. That is a trimer for K11V-TR and monomer for $K11V^{V4W}$-TR. Abeta at 0.5 µM was a positive control. The results were

normalized by using the buffer treated cell as 100% viability and cell treated with 0.2% SDS as 0% viability.

Preparation of Large Unilamellar Vesicles (LUVs)

Calcein-containing LUVs were prepared as described previously (19), with minor modifications. 1-palmitoyl-2-oleoyl-sn-glycero-3-phosphocholine (POPC) and 1-palmitoyl-2-oleoyl-sn glycero-3-phospho-L-glycerol (POPG) were obtained from Avanti Polar Lipids (Alabaster, AL). Mixtures of POPC and POPG in a 7:3 molar ratio were dissolved in 1:1 chloroform:methanol. The solvent was evaporated under dry nitrogen gas to yield a lipid film that was further dried under vacuum for at least 24 hours to remove any residual organic solvent. The film was then hydrated in 70 mM calcein (Sigma Aldrich, St. Louis, MO) and 10 mM Tris-HCl (pH 7.4) at a lipid concentration of 5 mM. The suspensions were subjected to 10 freeze-thaw cycles of temperatures of -80 and 50 °C, followed by extrusion through two 0.2 μm pore size filters (Whatman, Florham Park, NJ). Non-encapsulated calcein was separated from calcein-filled LUVs by size exclusion using a Sephadex G-75 (GE Healthcare, Piscataway, NJ) equilibrated in buffer (10 mM Tris-HCl pH 7.4, 100 mM sodium chloride). The calcein-containing LUVs were concentrated to 3-5 mM and stored at 4 °C. Phospholipid content and concentrations of the LUVs were determined by RP-HPLC using 100% Methanol and 100 mM TEAC (tetraethylammonium chloride) pH 7.8 as the solvent and a C18 column. Diameter of LUVs were determined using a Microtrac UPA 150 (York, PA). LUV preparations displayed diameters between 170-200 nm for at least 10 days. LUVs were used for experiments within 5 days of preparation.

Membrane Leakage Experiments

Pure, lyophilized K11V-TR and K11V^{V2L}-TR peptides were solubilized in water. Three different stock solutions were made at concentrations of 0.2, 0.8, and 2 mM. 5 uL of each peptide stock solution was added to a well containing 195 uL of 7:3 calcein-containing POPC:POPG LUVs in a buffer (10 mM Tris-HCL pH 7.4, 100 mM sodium chloride). Dye leakage was measured using a SpectraMax5 (Molecular Devices, Sunnyvale, CA) at 485 nm excitation and a 535 nm emission. Measurements were taken every 10 minutes for 30 hours. Each well contains a final LUV concentration of 100 μM with final K11V-TR and K11V^{V2L}-TR construct concentrations of 5, 20, and 50 μM. Synthetic human Islet Amyloid Polypeptide (hIAPP) residues 8-37, purchased from CS-Bio (Menlo Park, CA), was used as a positive control; since hIAPP has been previously shown to interact and disrupt membranes (*25, 26*). Lyophilized hIAPP was dissolved in 100% hexafluoro-2-propanol (HFIP) and put under vacuum to evaporate the HFIP. hIAPP was then reconstituted in water at 0.2 mM, filtered using a 0.2 μm filter, and added to six wells containing 100 μM Calcein-containing LUVs to a final concentration of 5 μM hIAPP. Fluorescence at a given time point was normalized as described previously (20), using the equation: $F_{normalized} = (F_t - F_{min})/(F_{max} - F_{min})$. F_t is the measured fluorescence intensity, F_{min} the fluorescence of 100 μM calcein-containing LUVs alone, and F_{max} is the maximum fluorescence determined by incubation of 100 μM LUVs in the presence of 0.5% Triton X-100.

SOM Text

Proposed and Similar Cylindrin Models

Considering conformational and geometrical properties of anti-parallel beta-sheets, Salemme and Weatherford attempted to model a six stranded barrel with a minimum of four interchain hydrogen bonds (*28*). They were unable to present a model, but observed one or more beta-bulges when maintaining beta-sheet twist, and a chain tendency to diverge at the ends of the barrel (*28*).

A Dali (*63*) and MATRAS (*64*) search was performed using the cylindrin as the search model to find similar structures. A cylindrin containing six chains, all with the same chain identification, was used to overcome the minimum chain length limit of 30 amino acids in Dali. The top scoring search result for Dali was alpha-amino acid ester hydrolase (PDB 1RRY) and for MATRAS was cytokine receptor common beta chain (PDB 1EGJ) residues 339-437. The Dali top result has a Z score of 2.7 and rmsd of 3.2, and MATRAS a Z score of 13.74. The MATRAS top scoring structure has the greater similarity, containing seven beta strands in a cylindrical type fashion. The Dali top scoring model has little similarity, and poor alignment to the alpha-amino acid ester hydrolase sequence, which may explain the low Z score of 2.7. Interestingly, a similar structure can be found in the PduU shell protein (PDB 3CGI), but not found using the above search engines. The PduU shell proteins N-termini form a six stranded parallel barrel (*65*). The parallel beta barrel, containing residues 7-17, has an Ab of 1050 $Å^2$ and Sc of 0.76. Exhibiting similar molecular properties to the anti-parallel cylindrin structure, we classify this as a parallel cylindrin. A similar beta barrel with a shear number of 6 has been observed in the tetrahydrodipicolinate-N-succinyltransferase protein (PDB 1TDT) (*66*). This barrel is formed from C-terminal hairpins of 3 chains, adopting an antiparallel structure. But unlike the cylindrin, the interior seems to be quite polar, containing H-bonded rings of Asn and Ser sidechains and some waters.

Cylindrin Crystal Packing

A different crystal packing was observed with the K11V-Br2 peptide, in which valine at position 2 is substituted by (2-bromoallyl)-glycine. In this derivatized structure, the asymmetric unit is two entire neighboring cylindrins. In contrast, cylindrins formed from the wildtype sequence K11V and the derivatized segment K11V-Br8, contain only one crystallographically unique cylindrin. The RMSD of the wildtype structure superimposed on the bromo-derivative structures is 0.76 and 0.37 Å for K11V-Br2 and K11V-Br8, respectively; RMSD of the wild-type backbone on the bromo-derivative backbones is 0.33 and 0.29 Å for K11V-Br2 and K11V-Br8, respectively.

Molecular Dynamic Simulations and Calculations

Molecular dynamics (MD) simulations were carried out to examine the structural transition pathway and the energetics associated with the conversion between the native conformation (cylindrin; Fig. S9A) and a cylindrin fibril model (discussed below; Fig. S9B). These two models are the two target structures used in the molecular simulation. NAMD software was used to integrate classical equations of motion of model systems

(*67*), and the Charmm22 all-atom force field with CMAP correction (*68*) was used. Van der Waals and electrostatic interactions were switched with a 12 Å cutoff distance. The SHAKE algorithm constrained the covalent bond length of a polar hydrogen atom to its donor, which enabled 2 fs integration step. The native model was solvated with TIP3 explicit water molecules in an 80 $Å^3$ cubic box. Initially each target conformation was energy minimized in 1200 steps, heated to 300 K in 100 ps and equilibrated in 500 ps by rescaling temperature periodically. During the equilibration and the production period, Langevin piston algorithm controlled the pressure at 1 atm and the temperature at 300 K. Next, we adopted targeted MD (TMD) simulation (*69*) to elucidate intermediate conformations in the middle of the transition pathway. After the equilibrating period, cylindrin was gradually transformed to the fibril model in 20 ns by applying a constraining potential on *Cα* atoms (forward simulation);

$$U(\vec{x},t) = \tfrac{1}{2}k\left(R(\vec{x}) - R^*(t)\right)^2$$

where $\vec{x}$ is the coordinate vector of *Cα* atoms, t is the current simulation time, k is strength of the constraint which was set to 20 kcal/mol/$Å^2$, $R(\vec{x})$ is the root-mean-squared deviation (RMSD) of *Cα* atoms to the β-sheet, and $R^*(t)$ is the target RMSD at t which was linearly reduced from the initial RMSD between two end structures (10.04 Å) to zero as the simulation progressed. We also performed a reverse TMD simulation starting from the last snapshot of the forward simulation, and gradually transformed the molecule to cylindrin (backward simulation). The TMD simulations successfully converted the cylindrin to the fibril and *vice versa*.

TMD simulation is susceptible to hysteresis effect in energy changes which hampers accurate estimation of free energy difference and the transition state energy between two end structures (*69*). Therefore we employed free energy perturbation (FEP) simulation aimed at an accurate estimation of the free energy change associated with the structural conversion from the cylindrin to the fibril model (*70, 71*). The relative difference in RMSD (*ΔRMSD*) of the two end structures was chosen as the reaction coordinate of the transition. The reaction coordinate varied from -10.0 Å to +10.0 Å, which was divided by 40 equally spaced windows. Initial conformers for the FEP simulation were chosen from the previous TMD simulation; for each window $i \in \{n \mid 1 \le n \le 40\}$, two of lowest energy conformation from each of the forward and the backward simulation were selected. We applied an umbrella potential to each initial conformation, whose energy minimum was located at the center of the window;

$$U_i(\vec{x},t) = \tfrac{1}{2}k\left(R_1(\vec{x}) - R_2(\vec{x}) - R_i^*\right)^2$$

where i is the index of windows, $R_1(\vec{x})$ and $R_2(\vec{x})$ are RMSD of *Cα* atoms to cylindrin and to the fibril model respectively, k is 20 kcal/mol/$Å^2$, and R_i^* is the offset of the umbrella potential aligned with the center of each bin. For each window, the initial conformation was heated to 300 K in 100 ps, while employing a harmonic constraint to *Cα* atoms to prevent abrupt structural changes. The Langevin piston algorithm was applied to maintain pressure at 1 atm with a temperature of 300 K. During the production period, the offset of the umbrella potential was shifted from *i* to *i+1*, *i*+1 to *i+2*, *i* to *i*-1 and *i*-1 to i-2 positions respectively. Simulation period at each offset value varied from

0.75 to 1.5 ns depending on convergence of the simulation. The total energy, constraining energy, and reaction coordinate were saved every 0.2 ps, and coordinates were saved every 2.0 ps.

After finishing the FEP simulation we generated an energy histogram of the entire FEP simulation, using weighted histogram analysis method (WHAM) (*72*). The energy density of state (DOS) information was utilized to compute Gibbs free-energy of each window along the reaction coordinate (*ΔRMSD*), which was plotted in Fig. 3A. The free energy of a reaction coordinate window (*i*) is defined:

$$F_i = \sum_{\alpha \in \{i\}} \Omega(E_\alpha + U_\alpha) e^{-\beta E_\alpha} dE$$

where α is index of snapshots, *E* and *dE* are discretized energy level and its width (2 kcal/mol), Ω is energy density of state, and *Uα* is constraining potential of the window. In addition, a hierarchical clustering algorithm was used to define a representative conformation of each reaction coordinate window. We used a *Cα* RMSD distance of 3.0 Å as the cutoff for defining a structural cluster. The first 3000 snapshots were analyzed for lowest free energy within each window. A representative configuration in the most populated cluster is plotted in Fig. 3A. For free energy and clustering analyses, we used the MD Analysis package (*73*) and the Scipy-cluster package (*74*).

The total free energy of cylindrin and the steric-zipper fibril model were compared within the Molecular Mechanics-Generalized Born/Surface Area approximation method (MM-GB/SA) (*75*). The Generalized-Born solvation model and the surface area dependent hydrophobic energy were incorporated as functions of the solvation effect. This technique has been successfully applied for comparing the energetic stability of amyloid fiber models (*76*). The cylindrin steric-zipper fibril model, consisted of a steric-zipper interface wherein the hydrophobic residues (Val 2, Val 4, and Val 8) buried within the bilayer forming the dehydrated interface (Fig. S10). This model was solvated in a tetragonal solvation box ($29.15 \times 100 \times 100$ Å^3). The *X* dimension of the solvation box was aligned parallel to the fiber axis, as to represent an infinitely long fiber. The model was heated and equilibrated in 600 ps at 300 K, and simulated for 10 ns without structural constraints. The coordinates were saved every 2 ps. The steric-zpper interface was intact during the simulation period. In contrast, the cylindrin was solvated in an $80 \times 80 \times 80$ Å^3 solvation box, and simulated for 10 ns. After completion of MD simulations, simulated snapshots were analyzed without solvent molecules and analyzed using an implementation of Generalized-Born solvation model in Charmm v31 (*77, 78*). In the GBSA approximation, the total free energy of a molecule is sum of individual contributions (*75*);

$$E_{Total} = E_{Int} + E_{vdW} + E_{Elec} + E_{GB} + E_{ASP},$$

where E_{int} is summation of covalent bonding energy terms (bond, angle, dihedral, improper dihedral, and CMAP correction), E_{vdW} is Van der Waals energy, E_{Elec} is vacuum electrostatic energy, E_{GB} is Generalized-Born solvation energy, E_{ASP} is surface area dependent hydrophobic energy, with a surface tension coefficient $\sigma = 5$ cal/mol/Å^2, S_{Trans} is translational entropy, and S_{Rot} is rotational entropy. The trans-rotational entropy of the steric-zipper fibril was set to zero, since it precipitates *in vitro*. Unlike the original

method, the vibrational entropic contribution was ignored which contributes only a small fraction to the total energy (*76*). The density of cylindrin was set to 1 mM/L, and any change in this density did not affect our conclusion qualitatively; for example, when the density is set to 1 nM/L resulted in $-TS_{Trans} = -4.83\,\text{kcal/mol}$. The MM-GB/SA analysis determined the steric-zipper fibril model has -5.2 kcal/mol/peptide lower free energy than the cylindrin (Table S4).

Potential Cylindrin A11 Epitopes

Because the polyclonal A11 antibody was affinity purified on an Abeta containing matrix (*79*), cylindrin and Abeta prefibrillar oligomers presumably share an epitope(s) that is also shared by other toxic oligomers which the A11 antibody recognizes. Several structural features are shared by our current models of cylindrin. They are the radius of the cylindrin, water mediated backbone H-bonds at the ends of the cylindrin, and helical grooves between side chains on the outside surface of the cylindrin. These grooves are akin to the linear grooves between side chains on the outside surface of steric zippers, but are more pronounced because the cylindrin side chains project from a convex surface of the cylindrin.

Fibril Model of the Cylindrin Sequence

Fourier transform infrared spectroscopy of cylindrin, K11V-TR dried fibrils display anti-parallel beta sheet characteristics. In the FTIR spectrum (data not shown) we observed peaks at 1628 cm^{-1} and 1685 cm^{-1}, characteristic of intermolecular and anti-parallel beta sheet (*80, 81*), respectively. Therefore, an anti-parallel model for cylindrin fibrils was constructed similar to that observed for short steric zippers (*19*), and subsequently used in targeted molecular dynamics simulation (discussed above).

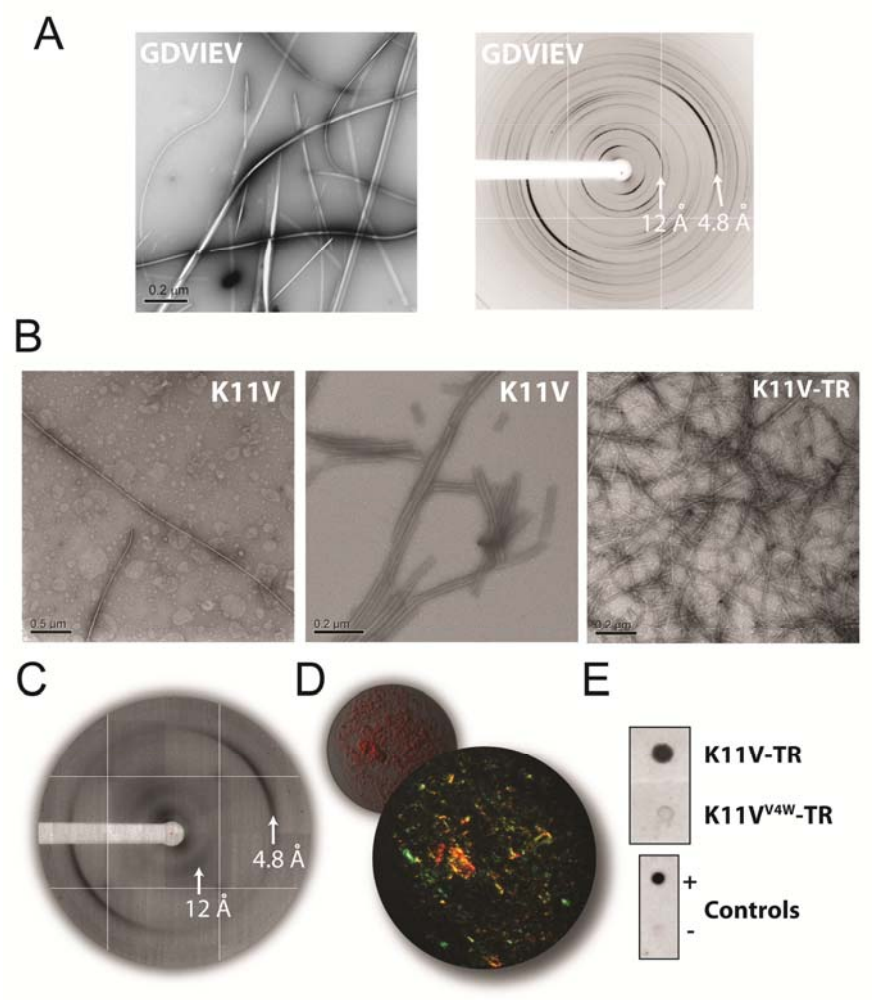

Fig. S1.

G6V (GDVIEV) and cylindrin peptides display amyloid biophysical characteristics. (**A**) Electron micrographs (EM) of negatively stained fibers formed by G6V (left side). Scale bar is shown. X-ray fibril diffraction pattern of dried G6V fibrils exhibit meridional reflections at 4.8 Å spacing and equatorial reflections at 12 Å (right side) spacing. Reflection rings are labeled. (**B**) Representative EM of various K11V-related peptides and their fibrils (described in methods). Cylindrin peptide abbreviations (see Table S1) and scale bar are shown. (**C**) X-ray powder diffraction pattern of K11V-TR fibrils, reflections are consistent with cross-beta sheet structure, as described for (A). (**D**) K11V-TR fibril sample was incubated with congo-red prior to drying on a cover slip (upper image). The fibrils are congo-red positive, displaying apple-green bifringerance under polarized light (lower image). (**E**) Immuno-dot blot analysis of solutions at equal concentration based on their oligomeric state of K11V-TR and negative control $K11V^{V4W}$-TR with polyclonal antibody, A11 (*5*). Positive control Abeta40 prefibrillar oligomers (+) and negative control Abeta40 fibrils (-) are shown.

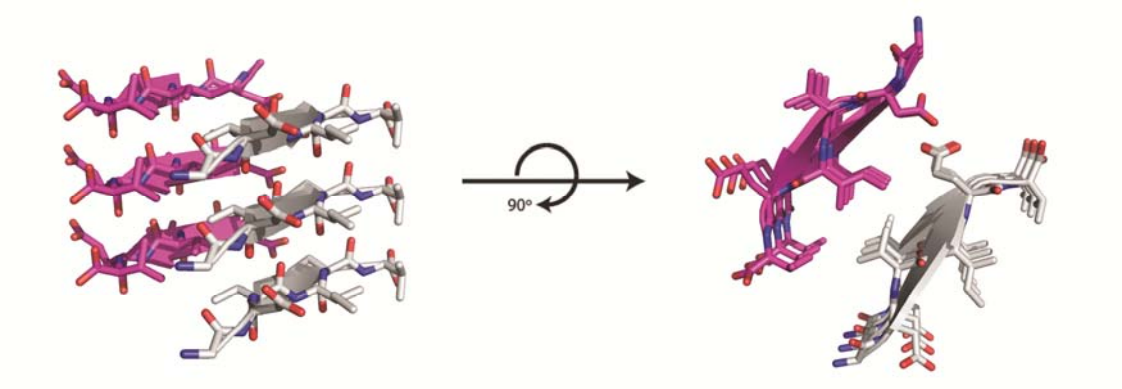

Fig. S2

Crystal structure of G6V (GDVIEV), the last six residues of the cylindrin peptide segment derived from alphaB crystallin (ABC). The segments form two parallel beta-sheets. The interface between the sheets is dry, containing no water. The aspartate residues form hydrogen bonds down the fibril axis (right).

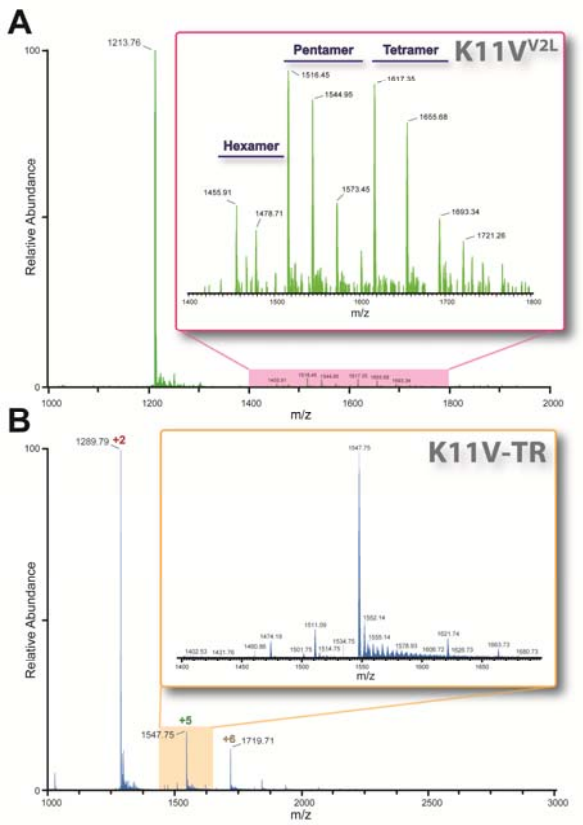

Fig. S3

Native nanoelectrospray mass spectrometry of K11V^{V2L} and K11V-TR oligomers. The cylindrin peptide abbreviation (see Table S1) is labeled for the respective mass spectrum in the upper right corner of the inset. (**A**) Mass spectrum of cylindrin peptide, K11V^{V2L} dissolved directly in 200mM ammonium acetate buffer. Expansion of the hexameric oligomers with *n*-1 and *n*-2 dissociation products (see for review (*62*)), shown in inset. The native ions 1455.91 and 1476.71 correspond to six peptide chains with a +5 charge state. The 1455.91 ion corresponds to a measured monoisotopic mass of 7270.4974 Da with a mass accuracy of 0.55 ppm. The *n*-1 (pentamer) and *n*-2 (tetramer) dissociated species are located under the respective label, corresponding to ions with +4 and +3 charge states, respectively. The 1231.76 ion corresponds to the K11V^{V2L} peptide chain with a +1 charge state. (**B**) Native mass spectrum of K11V-TR purified by size exclusion chromatography (see methods for details). The oligomer of three peptide chains, 1547.75 *m/z* with +5 charge state, has a measured monoisotopic mass of 7729.6852 Da with a mass accuracy of 3.93 ppm (Fig. 1D). The labeled +2 and +6 charge state ions correspond to one and four peptide chains, respectively. As only hexamers were observed for the single chain peptides, we suspected the K11V-TR tetramer may arise from non-specific aggregation during ion formation (see for review (*82*)). Native nanoelectrospray was performed on diluted samples of K11V-TR resulting in spectra with only trimers present (data not shown), being consistent with the higher order oligomers resulting from non-specific aggregation during ionization.

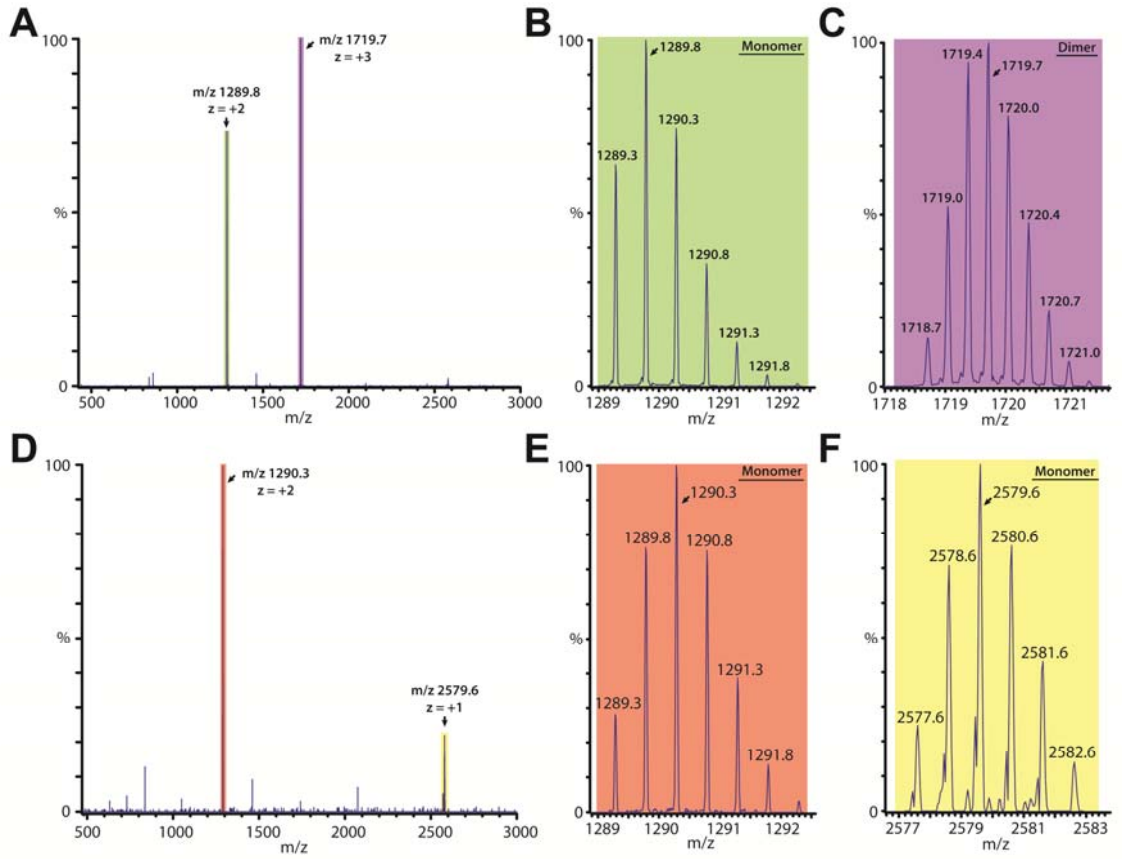

Fig. S4

Native nanoelectrospray mass spectrometry and collision induced dissociation (CID) of the K11V-TR cylindrin complex in the gas phase. (**A**) Ion isolation of the parent ion of 1548 of +5 charge (shown in figure 1D), corresponding to the oligomeric complex of three K11V-TR peptides, was subject to CID. The resulting dissociating products were a monomer and dimer corresponding to the ions of 1289 (shaded in green, zoom shown in panel **B**) and 1719 (shaded in purple, zoom shown in panel **C**), respectively. (**D**) Ion isolation of the +3 dimer ion of 1719 (panel A, shaded in purple) was subjected to CID. The dimer dissociated into monomeric units of +2 (shaded in orange, zoom shown in panel **E**) and +1 (shaded in yellow, zoom shown in panel **F**) charge. The K11V-TR cylindrin complex of three peptide chains in the gas phase followed charge state reduction into monomeric units, demonstrating the SEC-HPLC purified complex is composed of three peptides chains consistent with our crystal structures.

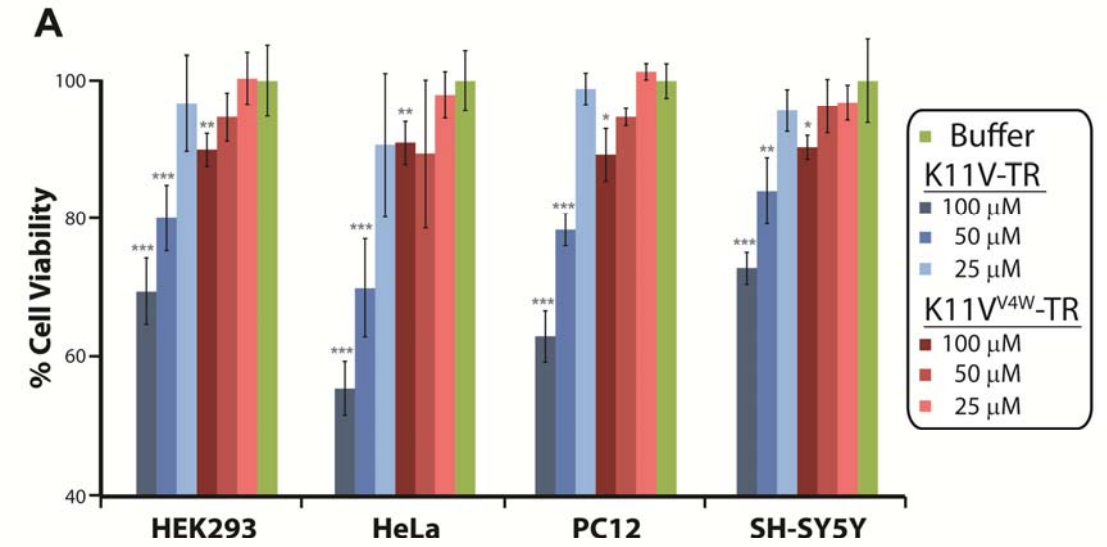

B

	Cell Line			
K11V-TR : K11V^{V4W}-TR	HEK293	HeLa	PC12	SH-SY5Y
100 μM	***	***	***	***
50 μM	***	*	***	**

Fig. S5

Cell toxicity of cylindrin peptides in HEK293, HeLa, PC12, and SH-SY5Y cell culture lines. (**A**) The cylindrin forming peptide, K11V-TR, displays concentration dependent cell toxicity in all four cell lines. The mutant cylindrin peptide, K11V^{V4W}-TR, designed to disrupt oligomer formation, show little to no cell toxicity. The cylindrin forming peptides in oligomeric form display cell toxicity, while the non-oligomer forming peptide displays no toxicity. Bars are color-coded for different peptide concentrations as shown in the figure legend on the right with cylindrin peptide abbreviations as listed in Table S1. Each bar represents the mean and SEM of twelve replicates from three independent tests. (**B**) A summary table of statistical significance for comparison of K11V-TR to the non-cylindrin forming peptide K11V^{V4W}-TR at similar peptide concentrations. Student's t-test ($N = 12$): *, $P < 0.05$; **, $P < 0.01$; and ***, $P < 0.001$.

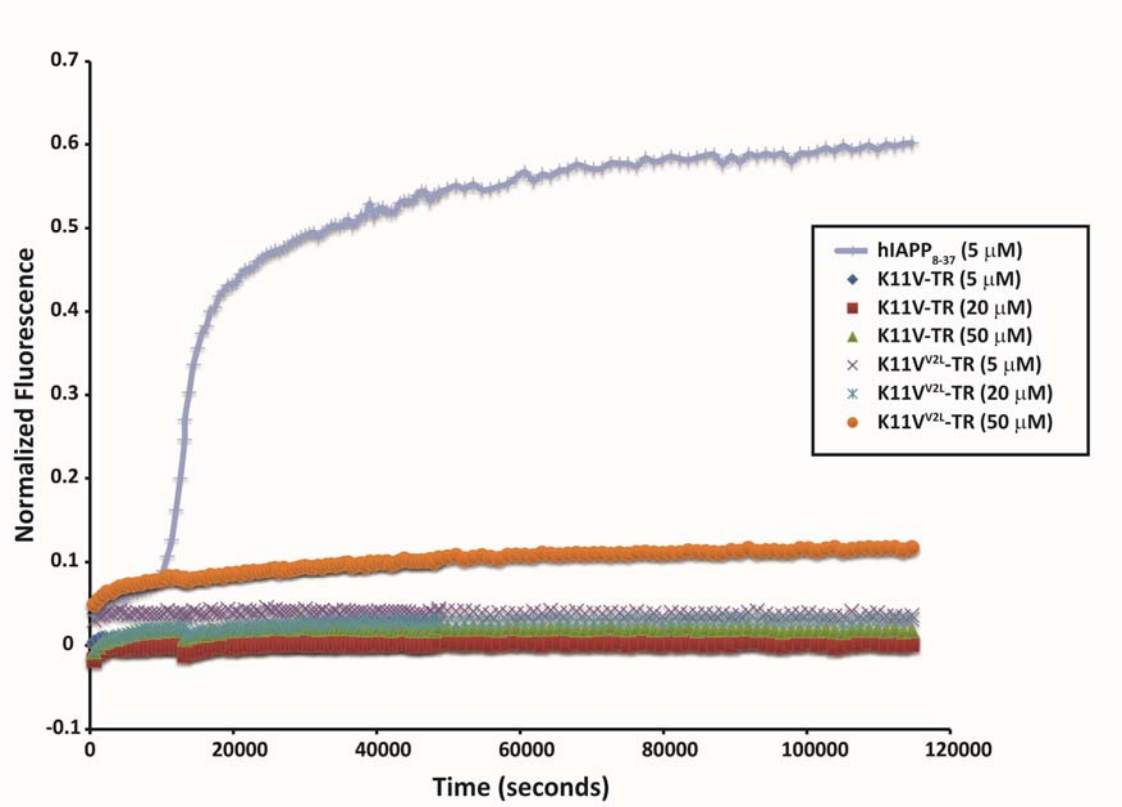

Fig. S6

Cylindrin tandem repeat peptides do not induce membrane leakage. Liposome dye-release experiments were performed with K11V-TR (wild-type), K11V^{V2L}-TR (contains V2L mutation in each repeat), or hIAPP$_{8-37}$ (residues 8-37) peptides. The concentrations used in experiments are shown (inset). Peptides were incubated with calcein-containing liposomes (details provided in experimental methods), and calcein fluorescence was measured over time. The hIAPP$_{8-37}$ was a positive control (*25, 26*), and leakage was observed up to 60%. The K11V-TR or K11V^{V2L}-TR peptides reached a maximum leakage of 10%, despite the concentration being 10 times higher compared to the hIAPP$_{8-37}$ peptide. This suggests that membrane disruption is not the main mechanism of toxicity for cylindrin.

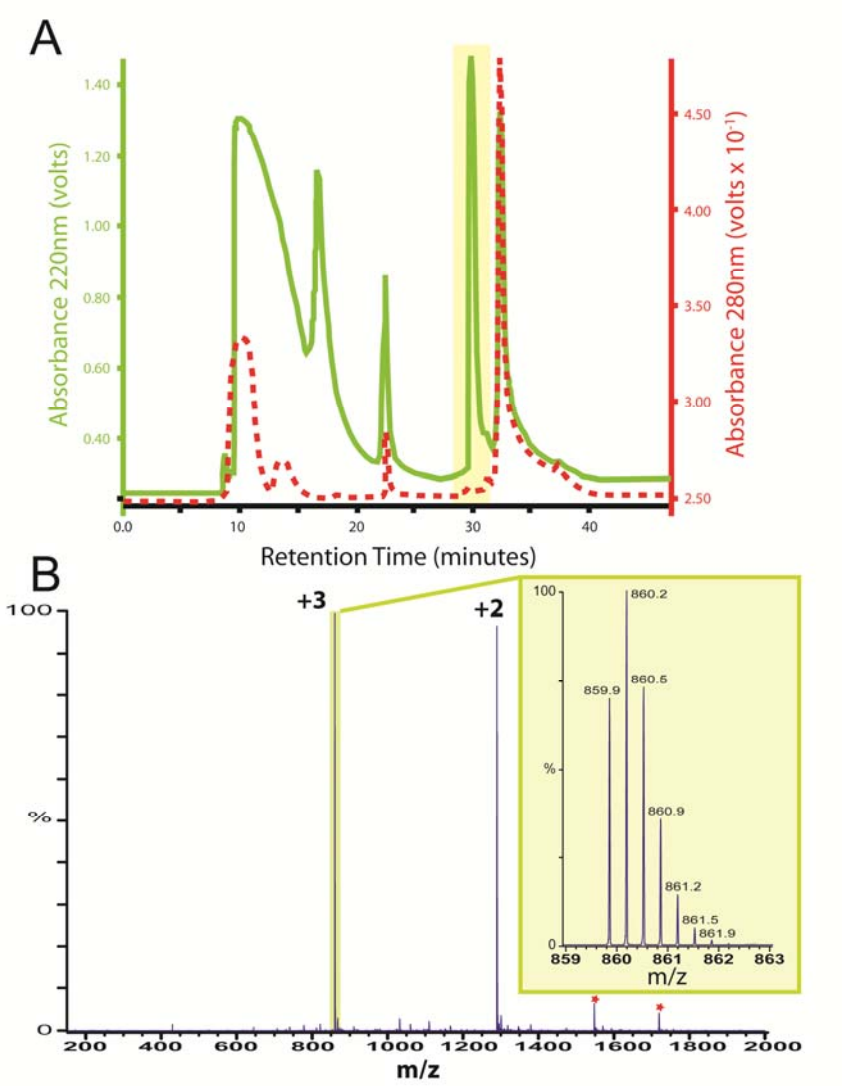

Fig. S7

Representative purification and purity of recombinant tandem repeat cylindrin peptides. (**A**) Reverse phase HPLC (RP-HPLC) chromatogram of tandem repeat cylindrin peptide, K11V-TR, post TEV protease treatment. Absorbance at 220nm and 280nm are shown by green and dashed red lines, respectively. The peak absorbing at 220nm corresponding to K11V-TR is highlighted by a shaded yellow box. Peak fractions were pooled and lyophilized. (**B**) Lyophilized peptide was dissolved in buffer (40% Acetonitrile, 0.1% TFA) and subject to nanoelectrospray mass spectrometry. The two most abundant ions, with charge states labeled, correspond to a molecular mass consistent with the K11V-TR peptide. Under these conditions ions of a +5 and +3 charge were observed, labeled by red stars, corresponding to oligomeric molecular masses consistent with three and two K11V-TR peptides, respectively.

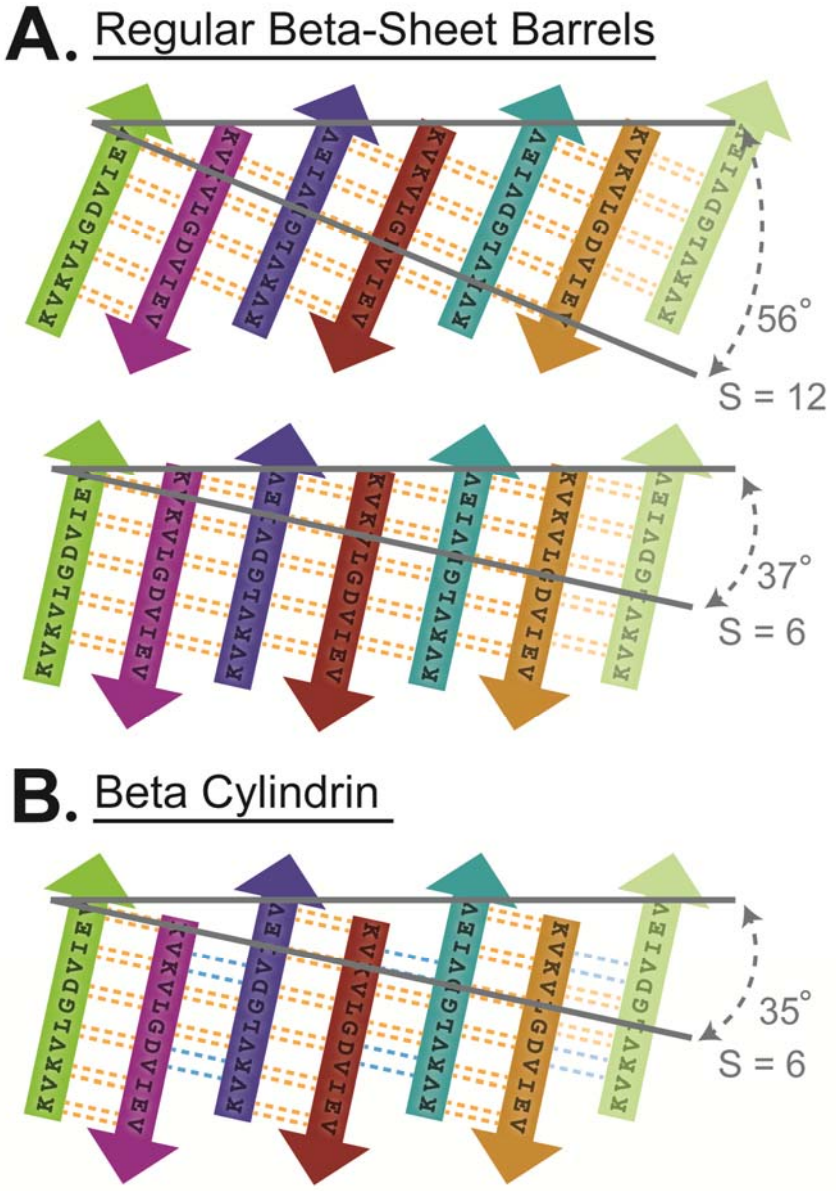

Fig. S8

Schematics of unrolled anti-parallel regular beta-sheet barrels and cylindrin. Shown in each schematic is shear number, S, and the mean slope of the strands to the central axis of the barrel, in degrees, as described by Murzin et al. 1994 (*33*), not drawn to scale. (**A**) For ideal regular beta barrels of six strands with a shear number of 12 and 6, the mean slope is 56° and 37° (*33*), respectively. Hydrogen bonds are shown by dashed yellow lines. (**B**) The cylindrin with a shear number of 6 has a mean slope of ~35°. Hydrogen bonds are shown as described in Fig. 2. The mean slope of cylindrin is similar to that for the regular S=6 mode, but the sheet-to-sheet offset and hydrogen bonding differ.

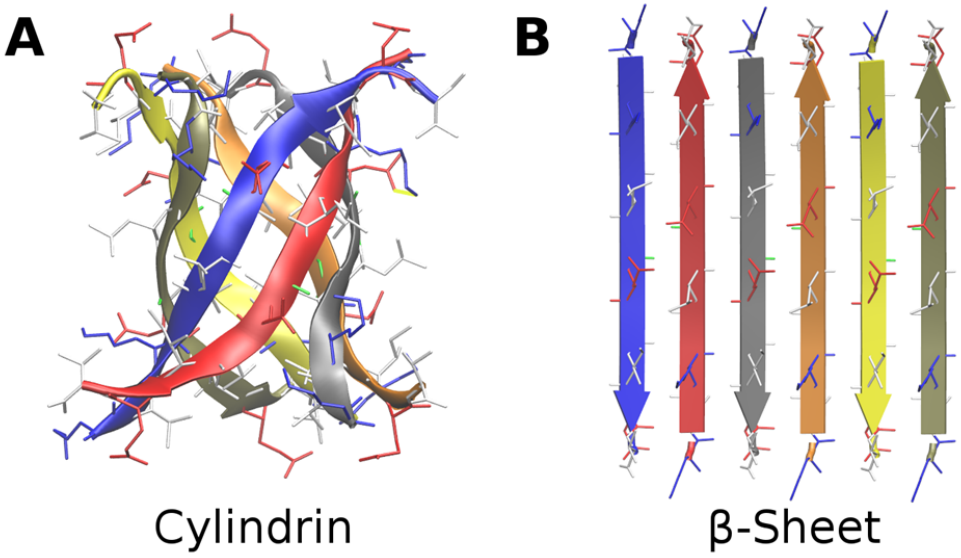

Fig. S9

The two reference structures used in the molecular dynamics simulations: (**A**) cylindrin and (**B**) cylindrin in-register anti-parallel beta sheet amyloid fibril model (only half modeled). The root mean squared deviation (RMSD) between these two structures is 10.5 Å.

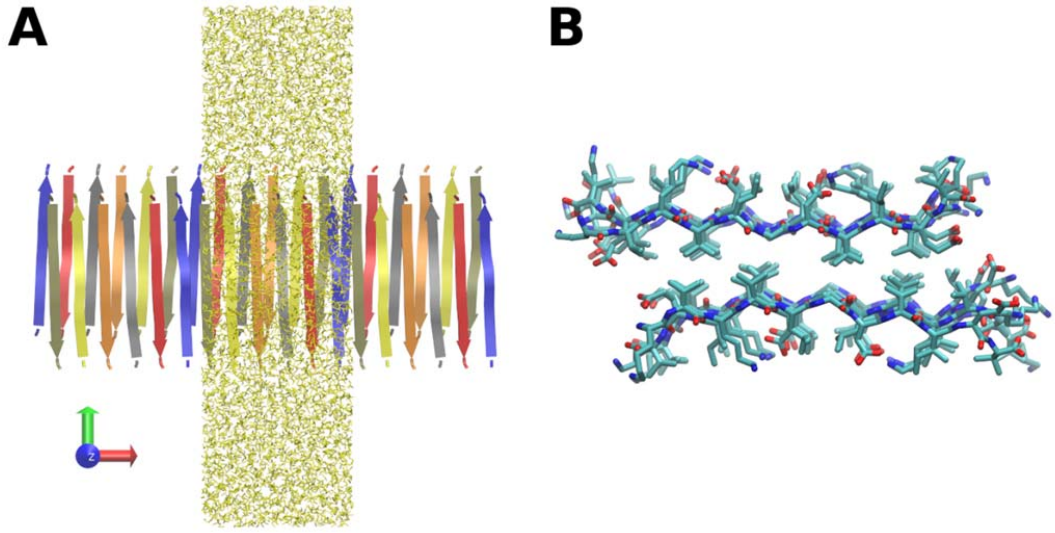

Fig. S10

MD simulation setup and fibril model of cylindrin, K11V. (**A**) The cylindrin in-register fibril model was placed in a periodic solvation box. (**B**) A snapshot of the bilayer after 10 ns MD simulation. The bilayer interface was dehydrated throughout the simulation period.

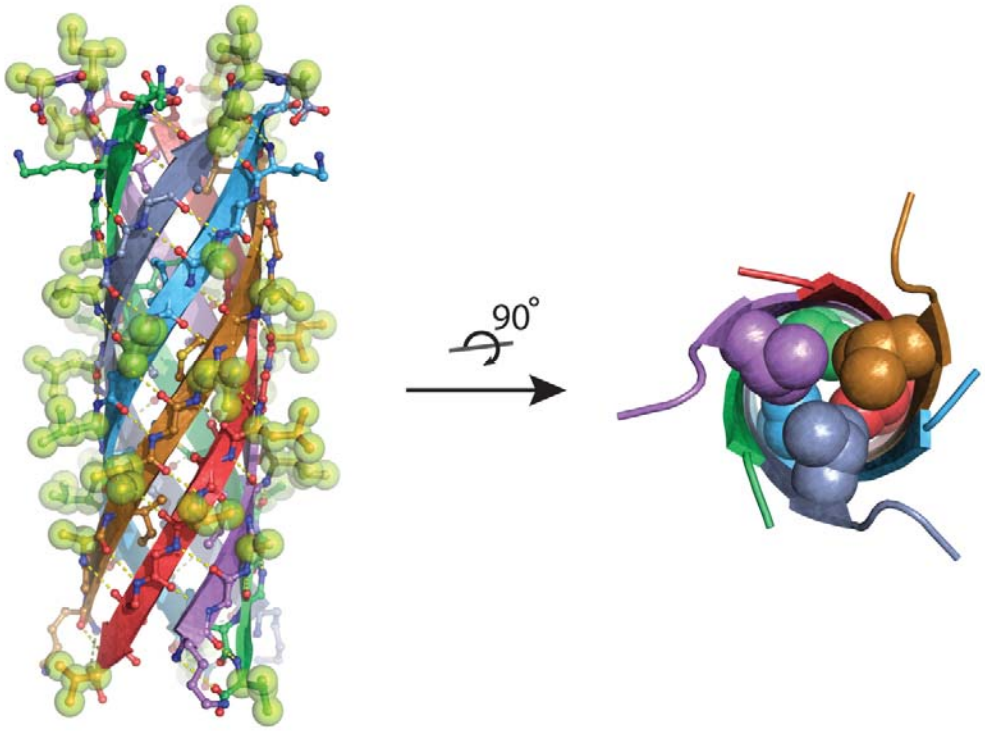

Fig. S11

Cylindrin-like model of Abeta, viewed both perpendicular to (left) and down (right) the cylindrin axis. This model, one of several possible, is built from three identical anti-parallel pairs of Abeta segments: Abeta(26-40) and Abeta(28-42). In the view perpendicular to the cylindrin axis, apolar sidechains are green. The view down the cylindrin axis shows apolar sidechains filling the cylinder.

Table S1.

Cylindrin single chain and tandem repeat peptide abbreviations and amino acid sequences.

Peptide Abbreviation	Peptide Sequence
G6V	GDVIEV
K11V	KVKVLGDVIEV
K11V-Br2	K*B*KVLGDVIEV
K11V-Br8	KVKVLGDV*B*EV
$K11V^{V2L}$	KLKVLGDVIEV
K11V-TR	GKVKVLGDVIEVGGKVKVLGDVIEV
$K11V^{V2L}$-TR*	GKLKVLGDVIEVGGKLKVLGDVIEV
$K11V^{V4W}$-TR	GKLKWLGDVIEVGGKLKWLGDVIEV

B – residue substitution with (2-bromoallyl)-glycine a non-natural amino acid;
* - This peptide sequence has been denoted as K11V-TR in the main text.

Table S2.
X-ray Data Collection and Refinement Statistics [a].

	K11V	K11V-Br2[b]	K11V-Br8[b]	K11V^{V2L}	K11V-TR	GDVIEV
Data Collection						
Synchrotron Beam line	APS 24-ID-C	ALS 8.2.1	APS 24-ID-C	APS 24-ID-C	APS 24-ID-C	APS 24-ID-E
Reflections observed	7,715	21,693	10,088	84,426	23,465	2,148
Unique reflections	973	6,043	1,509	9,431	6,428	438
Wavelength (Å)	0.97918	1.00	0.91963	0.9794	0.97918	0.97915
Resolution (Å)	2.55	1.62	2.8	1.4	2.16	1.7
Highest Resolution Shell (Å)	2.64-2.55	1.68-1.62	2.9-2.8	1.6-1.4	2.21-2.16	1.83-1.7
Space group	$I4_132$	$I2_13$	$I2_13$	$I2_13$	$P6_1$	$P2_1$
R_{sym} (%) [c]	7.5 (60)	3.3 (28.6)	9.0 (66.3)	7.2 (49.9)	4.5 (41.6)	17.8 (38.6)
I/σ	16.8 (1.6)	25.0 (3.2)	15.9 (2.5)	25.3 (3.1)	14 (3.7)	5.1 (5.0)
Completeness (%)	92 (98)	97.2 (98.7)	100 (100)	99.8 (100)	99.3 (4.7)	97.6 (100)
Unit cell dimensions						
a, b, c (Å)	69.2, 69.2, 69.2	65.9, 65.9, 65.9	70.3, 70.3, 70.3	65.8, 65.8, 65.8	52.34, 52.34, 87.33	4.8, 19.5, 21.0
α, β, γ (°)	90, 90, 90	90, 90, 90	90, 90, 90	90, 90, 90	90, 90, 120	90, 94.2, 90
Refinement						
Resolution (Å)	48-2.5	33-1.7	49-2.8	46-1.4	19.7-2.17	14-1.7
Reflections Used	914	5,409	1,373	9,412	6,421	389
R_{work}(%)	24.4 (38.5)	18.7 (17.1)	23.3 (24.5)	17.8 (19.7)	18.4 (22.0)	21.23 (29.2)
R_{free} (%)	26.9 (46.8) [d]	22.9 [d]	23.6 (37.4) [d]	24.0 (22.6) [d]	23.4 (25.5) [e]	22.4 (20.1) [e]
Peptides in Asymmetric Unit	1	4	2	4	6	1
Number of non-H atoms						
Protein	84	345	170	404	1,078	46
Non-protein	1	27	-	54	86	2
RMS deviations						
Bond lengths (Å)	0.022	0.012	0.016	0.007	0.01	0.011
Bond angles (°)	1.7	1.5	1.7	1.1	1.4	1.1
Average *B*-factor (Å^2)						
Protein atoms	40.8	20.6	71.0	19.6	63.8	9.2
Non-protein atoms	33.8	37.2	-	38.1	74.0	25.4
PDB accession code	3SGO	3SGM	3SGN	3SGP	3SGR	3SGS

[a] Highest resolution shell shown in parenthesis. [b] Number corresponds to position of (2-Bromoallyl)Glycine residue substitution in eleven amino acid peptide sequence, see Table S1. [c] $R_{sym} = \Sigma \mid I-\langle I\rangle \mid / \Sigma I$. [d] Rfree calculated using 5% of the data. [e] Rfree calculated using 10% of the data.

Table S3.
Surface area buried (SA) and surface complementarity (Sc) for cylindrin, G6V, and Sup35 peptide segment, GNNQQNY. Values for the fibril were calculated by using one chain buried within the extended fibril.

Peptide Segment	Structure Type	S_c	SA	SA/residue
K11V	Cylindrin	0.75	959	87
G6V	Two interacting strands	0.82	112	19
	Fibril	0.72	623	104
GNNQQNY	Two interacting strands	0.86/0.80*	147/157*	25/26*
	Fibril	0.82	787	131

*From Sawaya, *et al.* 2007 (*19*).

Table S4.

Results of GBSA calculations for cylindrin and fibril models at 300 K. The energy unit is kcal/mol/peptide.

Structure Type	E_{int}	E_{vdW}	E_{Elec}	E_{GB}	E_{ASP}	$-TS_{Trans}$	$-TS_{Rot}$	Total
cylindrin	164.8	-39.4	-179.7	-254.8	4.8	-3.68	-2.58	-310.6
fibril	172.6	-52.1	-410.6	-29.4	3.8	0	0	-315.7

Supporting References

51. D. M. Hoover, J. Lubkowski, *Nucleic Acids Res* **30**, e43 (May 15, 2002).
52. Z. Otwinowski, W. Minor, in *Methods in Enzymology,* Charles W. Carter, Jr., Ed. (Academic Press, 1997), vol. Volume 276, pp. 307-326.
53. W. Kabsch, *Acta Crystallogr D Biol Crystallogr* **66**, 125 (Feb, 2010).
54. T. Pape, T. R. Schneider, *Journal of Applied Crystallography* **37**, 843 (2004).
55. P. Emsley, K. Cowtan, *Acta Crystallogr D Biol Crystallogr* **60**, 2126 (Dec, 2004).
56. A. J. McCoy *et al.*, *J Appl Crystallogr* **40**, 658 (Aug 1, 2007).
57. G. N. Murshudov, A. A. Vagin, E. J. Dodson, *Acta Crystallogr D Biol Crystallogr* **53**, 240 (May 1, 1997).
58. P. D. Adams *et al.*, *Acta Crystallogr D Biol Crystallogr* **58**, 1948 (Nov, 2002).
59. B. Lee, F. M. Richards, **55**, 379 (1971).
60. M. C. Lawrence, P. M. Colman, *J Mol Biol* **234**, 946 (Dec 20, 1993).
61. *Acta Crystallogr D Biol Crystallogr* **50**, 760 (Sep 1, 1994).
62. H. Hernandez, C. V. Robinson, *Nat Protoc* **2**, 715 (2007).
63. L. Holm, S. Kaariainen, P. Rosenstrom, A. Schenkel, *Bioinformatics* **24**, 2780 (Dec 1, 2008).
64. T. Kawabata, K. Nishikawa, *Proteins* **41**, 108 (Oct 1, 2000).
65. C. S. Crowley, M. R. Sawaya, T. A. Bobik, T. O. Yeates, *Structure* **16**, 1324 (Sep 10, 2008).
66. N. Nagano, E. G. Hutchinson, J. M. Thornton, *Protein Sci* **8**, 2072 (Oct, 1999).
67. J. C. Phillips *et al.*, *J Comput Chem* **26**, 1781 (Dec, 2005).
68. A. D. Mackerell, Jr., M. Feig, C. L. Brooks, 3rd, *J Comput Chem* **25**, 1400 (Aug, 2004).
69. J. Schlitter, M. Engels, P. Kruger, *J Mol Graph* **12**, 84 (Jun, 1994).
70. N. K. Banavali, B. Roux, *J Am Chem Soc* **127**, 6866 (May 11, 2005).
71. J. Lee, Y. G. Kim, K. K. Kim, C. Seok, *J Phys Chem B* **114**, 9872 (Aug 5, 2010).
72. S. Kumar, J. M. Rosenberg, D. Bouzida, R. H. Swendsen, P. A. Kollman, *Journal of Computational Chemistry* **13**, 1011 (1992).
73. N. Michaud-Agrawal, E. J. Denning, T. B. Woolf, O. Beckstein, *J Comput Chem*, (Apr 15, 2011).
74. D. Eads. (2008).
75. W. Wang, P. A. Kollman, *J Mol Biol* **303**, 567 (Nov 3, 2000).
76. J. Park, B. Kahng, W. Hwang, *PLoS Comput Biol* **5**, e1000492 (Sep, 2009).
77. B. R. Brooks *et al.*, *J Comput Chem* **30**, 1545 (Jul 30, 2009).
78. W. Im, M. S. Lee, C. L. Brooks, 3rd, *J Comput Chem* **24**, 1691 (Nov 15, 2003).
79. R. Kayed, C. G. Glabe, *Methods Enzymol* **413**, 326 (2006).
80. M. Bouchard, J. Zurdo, E. J. Nettleton, C. M. Dobson, C. V. Robinson, *Protein Sci* **9**, 1960 (Oct, 2000).
81. H. Hiramatsu, T. Kitagawa, *Biochim Biophys Acta* **1753**, 100 (Nov 10, 2005).
82. J. L. Benesch, B. T. Ruotolo, D. A. Simmons, C. V. Robinson, *Chem Rev* **107**, 3544 (Aug, 2007).